Heat transport in active harmonic chains

Mei C. Zheng, Fred M. Ellis, and Tsampikos Kottos

Department of Physics, Wesleyan University, Middletown, Connecticut 06459, USA

Ragnar Fleischmann and Theo Geisel

Max-Planck-Institute for Dynamics and Self-organization, Am Faßberg 17, D-37077 Göttingen, Germany, and
Institute for Nonlinear Dynamics, Department of Physics, University of Göttingen, D-37077 Göttingen, Germany

Tomaž Prosen

Physics Department, Faculty of Mathematics and Physics, University of Ljubljana, Ljubljana, Slovenia

We show that a harmonic lattice model with amplifying and attenuating elements, when coupled to two thermal baths, exhibits unique heat transport properties. Some of these novel features include anomalous nonequilibrium steady-state heat currents, negative differential thermal conductance, as well as nonreciprocal heat transport. We find that when these elements are arranged in a $\mathcal{PT}$-symmetric manner, the domain of existence of the nonequilibrium steady state is maximized. We propose an electronic experimental setup based on resistive-inductive-capacitive (RLC) transmission lines, where our predictions can be tested.

I. INTRODUCTION

The study of heat transport and the investigation of new schemes for its control are some of the main challenges of statistical physics and thermal engineering. From the fundamental point of view, the challenge is to understand macroscopic phenomena and their statistical properties in terms of deterministic microscopic dynamics and in particular to connect macroscopic irreversibility with time-reversible microscopic evolution of a system of interacting particles. On the technological side, on the other hand, there is a lot of pressure to engineer high-efficiency thermoelectric materials and design efficient schemes for the control of heat transport. As a result, the study of heat transport in low-dimensional systems such as atom chains or various nanostructures has produced many exciting ideas [1–3], ranging from heat rectification [4] to heat logic gates [5]. In fact, some of these exciting theoretical suggestions recently have been experimentally realized [6]. Despite all this activity, our understanding of heat transport is far from being settled. For example, it is still not understood exactly what are the sufficient and necessary conditions in terms of microscopic dynamics for the validity of Fourier's law of heat conduction [7]. Even in linear (harmonic) oscillator chains, energy transport can have various features, depending on the (mass) disorder or spectral properties of the heat baths [3].

Until now, all the theoretical studies of energy transport on the nanoscale level have been conducted on *passive* (conservative) systems, that is, systems without any active elements which would amplify or dissipate local energy from or to some external degrees of freedom. However, dissipation mechanisms are inevitable in practical applications and thus one of the key challenges encountered in thermal engineering is their presence, which typically degrades the efficiency of thermal devices. As a result, considerable research effort is invested in eliminating and mitigating these undesirable absorption mechanisms. Below, we adopt the opposite viewpoint: by manipulating absorption and via a judicious design that involves the combination of amplification and absorption

regions, we achieve schemes of thermal conduction with intriguing properties similar to thermal rectification and heat switching. Our study is inspired by recent achievements in the field of optics, where it has been discovered [8] that a new class of synthetic materials (the so-called $\mathcal{PT}$ metamaterials) created by a delicately balanced arrangement of amplification and absorption regions can exhibit novel properties [8–10]. At the heart of these innovative ideas is the observation that non-Hermitian Hamiltonians, which respect the combined parity ($\mathcal{P}$) and time ($\mathcal{T}$) reversal symmetry, can have real spectrum and thus generate a (pseudo)unitary time evolution [11–13].

In this paper, we present a theoretical study of heat transport through an active harmonic chain coupled at the left and right edges to a pair of Langevin heat reservoirs with temperatures T_L and T_R respectively. For simplicity, we assume only one amplifier and one attenuator, which are placed on the left and right symmetrically with respect to the center of the chain. We show that such structures exhibit intriguing thermal transport characteristics. Associated separately with the left and right baths are critical values of the amplification and attenuation parameter, γ_L^* and γ_R^*, where the differential conductance changes sign, passing through zero. At either of these points, the heat flow into the bath is independent of its own temperature and is proportional only to the temperature of the other bath. Most remarkably, these critical values occur before the system reaches an instability point γ_i. The maximum size of the stability regime $\gamma < \gamma_i$ occurs at the exact balance of the gain and loss—the condition required for the $\mathcal{PT}$ symmetric Hamiltonian of an isolated chain. Finally, we propose an electronic experimental setup based on resistive-inductive-capacitive (RLC) transmission lines, where our predictions can be tested.

II. MODEL AND MATHEMATICAL FORMALISM

The mathematical model is schematically depicted in Fig. 1(a). It consists of a chain of $N = N_a + 2N_b$ particles
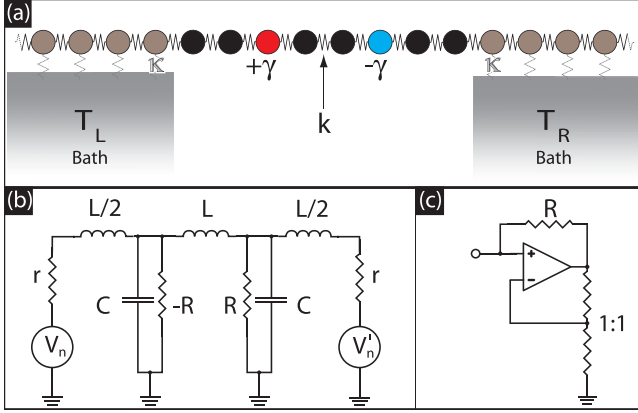
FIG. 1. (Color online) (a) Schematic illustration of an active harmonic chain model: $N_a = 8$ harmonic masses are coupled to two other large sublattices, which are in turn coupled to Langevin baths. (b) Electronic implementation of a simplified $N_a = 2$ (dimer) chain. The negative resistance gain element is provided by the operational amplifier (op-amp) negative impedance converter shown in (c). The voltage sources V_n and V_n' are synthesized noise generators, which along with the fixed r stand in for the thermal baths.

of equal mass m coupled by harmonic springs of constant k. The first (last) N_b particles are coupled to a Langevin reservoir of temperature T_L (T_R). We assume that the coupling constant κ with the reservoirs is the same for all particles. We also have two active oscillators, an amplifier (where the motion is linearly amplified), and an attenuator (where it is linearly damped) placed symmetrically with respect to the middle of the chain, at positions n_γ and $n_{-\gamma}$ respectively. An electronic realization shown in Fig. 1(b) is discussed at the end of this paper.

Using units in which $m = k = 1$, the corresponding stochastic equations of motion are

$$
\begin{aligned}
dq_n/dt &= p_n; \quad n = 1, \ldots, N, \\
dp_n/dt &= q_{n+1} - 2q_n + q_{n-1} + \sum_{\sigma = \pm} \sigma\gamma \delta_{n, n_{\sigma\gamma}} p_n \\
&\quad + \sum_{\tau = L, R} (-\kappa p_n + \sqrt{2\kappa T_\tau}\xi_n)\theta_n^\tau,
\end{aligned} \tag{1}
$$

with open boundaries $(q_0 \equiv q_{N+1} \equiv 0)$, $\theta_n^L = \{1 \text{ if } n \leqslant N_b;\ 0 \text{ otherwise}\}$, $\theta_n^R = \{1 \text{ if } n > N_a + N_b;\ 0 \text{ otherwise}\}$, $\xi_n(t)$ being δ-correlated Gaussian stochastic variables with $\langle \xi_n(t)\xi_{n'}(t')\rangle = \delta_{n, n'}\delta(t - t')$ where the bracket represents a noise average.

For $\kappa = 0$, the system of N coupled oscillators is isolated from the reservoirs. In this case, the Hamiltonian associated with Eqs. (1) is $\mathcal{PT}$ symmetric [11]. The normal modes and eigenfrequencies can be calculated by performing the substitution $q_n^\alpha = A_n \exp(\lambda_\alpha t)$. In accordance to the standard $\mathcal{PT}$ scenario [11,14], we find that the eigenfrequencies λ_α are imaginary for an amplification and attenuation parameter γ smaller than a critical value $\gamma_{\mathcal{PT}}$. In this regime, the normal modes are also eigenmodes of the $\mathcal{PT}$ operator. For $\gamma > \gamma_{\mathcal{PT}}$, the eigenfrequencies of the system are complex, while the normal modes are no longer eigenstates of the $\mathcal{PT}$ operator.

For $\kappa \neq 0$, we use Ito calculus of stochastic differential equations and derive the equation of motion for the covariances $\mathbf{C}(t) = \langle \vec{x}(t) \otimes \vec{x}(t)\rangle$, where the vector $\vec{x}$ is defined as $\vec{x} = (q_1, \ldots, q_N, p_1, \ldots, p_N)^T$. We find [2,3]

$$
d\mathbf{C}/dt = \mathbf{Z}\mathbf{C} + \mathbf{C}\mathbf{Z}^T + \mathbf{Y}, \tag{2}
$$

where $\mathbf{Z}$ and $\mathbf{Y}$ are $2N \times 2N$ matrices

$$
\mathbf{Z} = \begin{pmatrix} \mathbf{0} & \mathbf{1} \\ \mathbf{D} & \mathbf{0} \end{pmatrix} + \sum_{\sigma = \pm} \sigma\gamma \mathbf{P}_{N+n_\sigma} - \sum_{\tau = L, R} \mathbf{Y}^\tau, \tag{3}
$$

$$
\mathbf{Y} = \sum_\tau T_\tau \mathbf{Y}^\tau, \quad \text{with} \quad \mathbf{Y}^\tau = \kappa \sum_{n=1}^N \theta_n^\tau \mathbf{P}_{N+n}. \tag{4}
$$

Above, $\mathbf{P}_k = \vec{e}_k \otimes \vec{e}_k$ are diagonal rank 1 projectors, $\vec{e}_k$ is a basis vector with elements $(\vec{e}_k)_n = \delta_{n, k}$, and $\mathbf{D}$ is an $N \times N$ matrix with elements $D_{n, m} = -2\delta_{n, m} + \delta_{n, m+1} + \delta_{n, m-1}$ which encodes all the physical information about the interactions within the harmonic lattice.

III. THEORETICAL ANALYSIS

We are interested in the *nonequilibrium steady state* (NESS), whose covariance matrix $\mathbf{C}^\infty$ satisfies the Lyapunov equation [2,3]

$$
\mathbf{Z}\mathbf{C}^\infty + \mathbf{C}^\infty \mathbf{Z}^T = -\mathbf{Y}. \tag{5}
$$

The existence and the stability of the NESS are determined by the (complex) spectrum $\{\lambda_\alpha, \alpha = 1, \ldots, 2N\}$ of the real nonsymmetric matrix $\mathbf{Z}$,[1] defining a biorthonormal set of right $\vec{v}_\alpha$ and left $\vec{v}_\alpha'$ eigenvectors,

$$
\mathbf{Z}\vec{v}_\alpha = \lambda_\alpha \vec{v}_\alpha, \quad \mathbf{Z}^T \vec{v}_\alpha' = \lambda_\alpha \vec{v}_\alpha', \quad \vec{v}_\alpha \cdot \vec{v}_\beta' = \delta_{\alpha, \beta}. \tag{6}
$$

In other words, NESS exists if all eigenvalues λ_α have *negative real part*, $\text{Re}\lambda_\alpha < 0$. Otherwise, if for some α, $\text{Re}\lambda_\alpha > 0$, the time-dependent covariances (2)—for a generic initial condition—increase as $\exp(2t\text{Re}\lambda_\alpha)$, signaling an uncontrolled amplification of the system.

The transition to unstable behavior is determined by the parameter γ. We define γ_i as the point for which the first eigenvalue reaches the imaginary line $\text{Re}\lambda_1(\gamma = \gamma_i) = 0$. In Fig. 2(a), we show the parametric evolution of $\text{Re}\lambda_\alpha$ as a function of γ for the $\mathcal{PT}$ configuration of Fig. 1. We note that most of the eigenvalues are located inside a band and remain unchanged as γ increases. Only a single pair of eigenvalues $\lambda_{1,2}$ is approaching and crossing the imaginary line at $\gamma = \gamma_i$. This is remnant of the spontaneous $\mathcal{PT}$-symmetry-breaking scenario appearing in isolated systems. In Figs. 2(b)–2(e), we further compare the behavior of $\lambda_{1,2}(\gamma)$ for various coupling constants κ and degrees of asymmetry between $\gamma_L = \gamma$ and $\gamma_R = -\gamma(1 - \Delta)$. We find that the $\mathcal{PT}$ configurations (corresponding to $\Delta = 0$) result in the largest value of $\gamma_i \approx \gamma_{\mathcal{PT}}$ [see Fig. 2(b)]. A perturbative argument in κ, whose validity was checked numerically, allows us to better understand the behavior of $\text{Re}\lambda_{1,2}(\gamma)$: For $\kappa = 0$, both $\lambda_{1,2}(\gamma)$

---

[1]We order the eigenvalues with regard to the nonincreasing real part $\text{Re}\lambda_\alpha \geqslant \text{Re}\lambda_\beta$ for $\alpha < \beta$. Moreover, since $\mathbf{Z}$ is real, the corresponding eigenvalues come in complex conjugate pairs $\lambda_{2k} = \lambda_{2k-1}^*$.
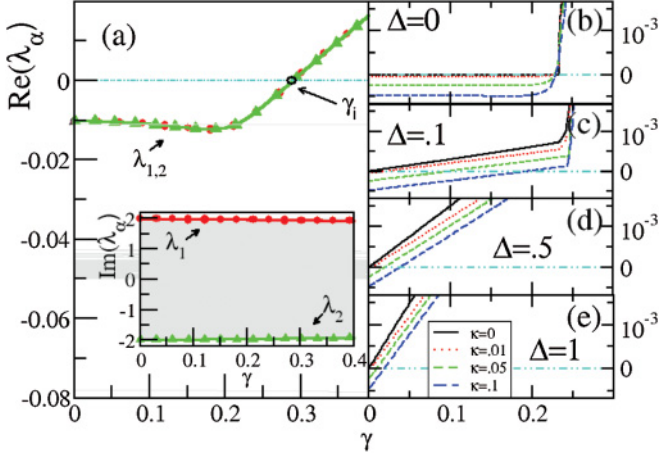
FIG. 2. (Color online) The real (a) and the imaginary [inset of (a)] part of the spectrum λ of the $\mathcal{PT}$-symmetric harmonic chain of Fig. 1(a) with $N_b = 50$ and $\kappa = 0.1$, vs the amplification and attenuation parameter γ. The green triangles (red circles) correspond to the leading eigenvalue, λ_1 (λ_2). (b)–(e) Parametric evolution of $\mathrm{Re}\lambda_{1,2}$ for the chain of Fig. 1 with $N_b = 1$, various κ values, and $\gamma_L = \gamma$, $\gamma_R = -\gamma(1 - \Delta)$. In case of $\Delta = 0$ [i.e., $\mathcal{PT}$-symmetric structure shown in panel (b)], γ_i is almost insensitive to κ and very close to $\gamma_{\mathcal{PT}}$ associated to $\kappa = 0$. As Δ increases [panels (c)–(e)], γ_i tends to zero.

FIG. 3. (Color online) (a) Heat flux J_L as a function of the parameter γ for various T_L temperatures and fixed $T_R = 10$; (b) heat flux J_R for various T_R temperatures and fixed $T_L = 10$. In the inset, we show a magnification of the area around γ_R^*. The dashed blue lines correspond to heat fluxes for the case where $T_L = T_R$. A nonreciprocal behavior is obvious.

increase linearly as a function of γ (for small γ values), with a slope $S \sim \Delta$. Increasing the coupling κ leads to a global shift of the eigenvalues (by an amount κ) toward the negative-real semiplane; that is, $\mathrm{Re}\lambda_{1,2}(\gamma) \sim -\kappa + S\gamma$. Consequently, we have that $\gamma_i \approx \min\{\kappa/S; \gamma_{\mathcal{PT}}\}$.

Our formalism can be utilized to derive the properties of NESS. For example, the energy current at site n is a linear combination of covariance matrix elements; that is,

$$J_n = \langle p_n(q_{n+1} - q_{n-1})\rangle = C_{n+1,n+N} - C_{n-1,n+N}. \quad (7)$$

Furthermore, since the matrix $\mathbf{Y}$ on the right-hand side of Eq. (5) is *linear* in the two bath temperatures T_τ, its solution— the full covariance matrix—and hence all the currents are also linear in T_τ, namely

$$\mathbf{C}^\infty = T_L\mathbf{C}^L + T_R\mathbf{C}^R, \quad (8)$$

where $\mathbf{C}^\tau$ solve the *temperature-independent* Lyapunov equations $\mathbf{Z}\mathbf{C}^\tau + \mathbf{C}^\tau\mathbf{Z}^T = -\mathbf{Y}^\tau$. If J_L and J_R designate the energy and heat currents in NESS to the left and right baths respectively, that is, $J_L = J_n^\infty$ for $N_b < n < n_{\sigma\gamma}$ and $J_R = J_n^\infty$ for $n_{\sigma\gamma} < n \leqslant N_a + N_b$ (since J_n^∞ is site independent for passive sites uncoupled from the baths due to energy conservation), then we may write

$$J_\tau = K_L^\tau T_L + K_R^\tau T_R, \quad (9)$$

where $K_{\tau'}^\tau \equiv \partial J_\tau/\partial T_{\tau'}$ are temperature-independent coefficients obtained explicitly combining (8) and (9).

For $\gamma = 0$, clearly $J_L = -J_R$ and $K_L^L > 0$, $K_R^R < 0$. However, for an active system, a critical γ_τ^*, $0 < \gamma_\tau^* < \gamma_i$, may exist for which one of the currents J_τ does not depend on the corresponding temperature T_τ and thus the *differential thermal conductance* vanishes $K_\tau^\tau|_{\gamma=\gamma_\tau^*} = 0$. This is nicely illustrated
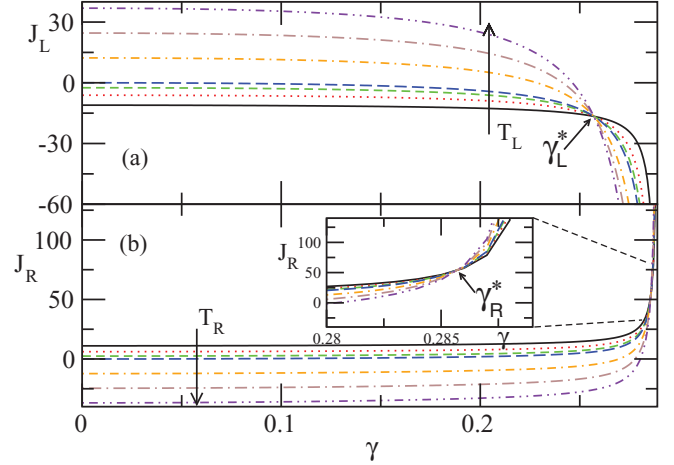
by our numerical data in Fig. 3. Moreover, as γ increases above γ_τ^*, the differential thermal conductance K_τ^τ changes sign. Specifically, we found that $K_L^L(\gamma < \gamma_L^*) > 0$ [$K_R^R(\gamma < \gamma_R^*) < 0$] while $K_L^L(\gamma > \gamma_L^*) < 0$ [$K_R^R(\gamma > \gamma_R^*) > 0$]. Thus, in the interval $\gamma_L^* < \gamma < \gamma_R^*$, both differential thermal conductances K_L^L, K_R^R are negative. While for $\gamma < \gamma_\tau^*$ the heat flow is consistent with the standard expectations, the opposite limit of $\gamma > \gamma_\tau^*$ is counterintuitive. Specifically, we find that $J_L < 0$, indicating flux toward the left bath, even if its temperature is higher than the one of the right bath, that is, $T_L > T_R$ [see Fig. 3(a)]. In fact, as T_L becomes higher, the magnitude of the heat flux $|J_L|$ becomes larger toward the left bath. Indeed, an increase of T_L results in stronger amplification of the local energy of the site n_{+-}, which will act as an effective bath with temperature $T_{n_+} = \langle p_{n_+}^2 \rangle$ higher than T_L (see also the right panels of Fig. 4). A similar argument can be used in order to understand the anomalous heat transport for the right flux J_R, that is, the flux measured closer to the attenuating oscillator n_-. In this case, the role of the attenuator is to shift γ_R^* to higher values compared to γ_L^*. This is illustrated in Fig. 3(b), where it is shown that higher T_R ($> T_L$) values lead to larger heat fluxes J_R.

We can use a further analytical approximation to get a general estimation of NESS in the vicinity $\delta\gamma = \gamma_i - \gamma$ of the instability point γ_i. We first note that the solution of the Lyapunov equation can be written in terms of a linear problem for the superoperator $\hat{S}$ acting on the matrix space of $2N \times 2N$ matrices $\mathbf{X}$, as $\hat{S}\mathbf{X} = \mathbf{Z}X + X\mathbf{Z}^T$. Specifically, $\hat{S}\mathbf{C}^\infty = -\mathbf{Y}$ or $\mathbf{C} = -\hat{S}^{-1}\mathbf{Y} = -\sum_\tau T_\tau\hat{S}^{-1}\mathbf{Y}^\tau$. Next, we define the two sets of matrices $\mathbf{V}_{\alpha,\beta} = \vec{v}_\alpha \otimes \vec{v}_\beta$ and $\mathbf{V}'_{\alpha,\beta} = \vec{v}'_\alpha \otimes \vec{v}'_\beta$, which are biorthonormal with respect to a matrix dot product $(\mathbf{A},\mathbf{B}) = \mathrm{tr}\mathbf{A}^T\mathbf{B}$, that is, $(\mathbf{V}_{\alpha',\beta'},\mathbf{V}_{\alpha,\beta}) = \delta_{\alpha,\alpha'}\delta_{\beta,\beta'}$. The latter identity can be easily derived with the help of Eq. (6). Using the above relations, we find the spectral decomposition for the superoperator $\hat{S}$, which reads as $\hat{S}\mathbf{V}_{\alpha,\beta} = (\lambda_\alpha + \lambda_\beta)\mathbf{V}_{\alpha,\beta}$. This
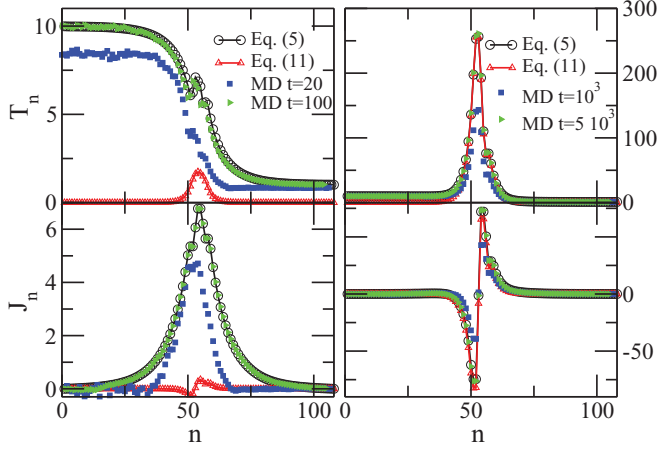
FIG. 4. (Color online) Flux and temperature profiles for two different situations of a chain with $N_a = 8$ and $N_b = 50$ sites. The bath temperatures are $T_L = 10$, $T_R = 1$, while the coupling to the bath is $\kappa = 0.1$: Left plots correspond to $\gamma = 0.1$, far away from the critical value $\gamma_i = 0.289$, while the right plots are for $\gamma = 0.286$, much closer to γ_i. The black curves correspond to the exact solution of Eq. (5), while the red curves (triangles) are associated with the analytical approximation Eq. (11). The blue (square) and green (right triangle) curves are results of the molecular dynamics (MD) simulations for various times. A nice convergence toward the theoretical predictions can be seen already for times $t = 100$ for $\gamma = 0.1$ and $t = 5 \times 10^3$ for $\gamma = 0.286$.

relation, together with the biorthonormality, allows us to derive a Liouvillean decomposition of the covariances

$$\mathbf{C}^\tau = -\sum_{\alpha, \beta} \frac{\vec{v}'_\alpha \cdot \mathbf{Y}^\tau \vec{v}'_\beta}{\lambda_\alpha + \lambda_\beta} \mathbf{V}_{\alpha, \beta}. \qquad (10)$$

Equation (10) is a very useful approximation in the vicinity of γ_i (i.e., for small $\delta\gamma$), since then, in our case (see Fig. 2), only a single pair of eigenvalues $\lambda_{1,2}$ dominates. By writing $\lambda_{1,2} \approx -\rho\, \delta\gamma \pm i\Omega$ where $\rho = -\partial \mathrm{Re}\lambda_{1,2}/\partial\gamma|_{\gamma_i}$, we have

$$\mathbf{C}^\tau = (\rho\, \delta\gamma)^{-1}(\vec{v}'_1 \cdot \mathbf{Y}^\tau \vec{v}'_2)(\mathbf{V}_{1,2} + \mathbf{V}_{2,1})/2 + \mathcal{O}[(\delta\gamma)^0]. \quad (11)$$

Equation (11) together with Eq. (7) yields an approximate expression of the current J_n near γ_i:

$$J_\tau = (1/\delta\gamma)\big(\mathcal{K}_L^\tau T_L + \mathcal{K}_R^\tau T_R\big) + \mathcal{O}[(\delta\gamma)^0], \qquad (12)$$

where $\mathcal{K}_{\tau'}^\tau$ are γ and temperature-independent coefficients. The divergence $J_\tau \sim 1/\delta\gamma$ is nicely seen in Fig. 3.

To further strengthen the validity of our approximations for the covariant matrix Eq. (11), we have calculated the temperature profile $T_n \equiv \langle p_n^2 \rangle = C_{N+n, N+n}$ and the current profile defined by Eq. (7). In Fig. 4, we compare the outcome of Eq. (5) with the predictions of Eq. (11) and find an excellent agreement as $\delta\gamma \to 0$.

We have also tested the accuracy of our theoretical calculations by comparing them with the outcomes of the direct molecular dynamics (MD) simulations for the system of Eqs. (1). In Fig. 4, we report the outcome of our simulations for two different γ values. In order to check the convergence of the MD simulations toward the theoretical results of Eq. (5), we have compared the temperature profile T_n and the flux J_n

for two different times in each of the γ cases (the time t is measured in units of inverse coupling). For γ values away from the γ_i this convergence is achieved quickly, while in the opposite case of $\gamma \to \gamma_i$ one needs to integrate Eq. (1) for much longer times. The MD results are averaged over an ensemble of 100 different bath configurations while the initial conditions of the displacement and momenta of the oscillators was in all cases taken to be $(q_n, p_n) = (0,0)$. An additional time average (over the last 20 time units) was performed in order to average out the oscillations of the chain elements. A convergence toward the theoretical results of Eq. (5) is evident.

IV. ELECTRONIC IMPLEMENTATION

We propose an RLC circuit [Figs. 1(b) and 1(c)] capable of demonstrating the qualitative features of the active harmonic lattice. The heat baths are implemented by synthesized noise sources V_n and V_n' having spectral density functions $S(\omega) = \frac{2}{\pi} k_B T r \sqrt{1 - \omega^2 LC/4}$, with a fixed series resistance $r = \sqrt{L/C}$ and T being the respective bath temperature. This spectral density along with the $L/2$ coupling into the ends of the system closely matches the Langevin reservoir of our lattice model. Moreover, the linear nature of the system allows for a computational correction of both the spectral function and impedance of the experimental bath to the infinite chain equivalent. The active lattice chain has an electronic equivalence to an RLC chain with the voltage on the capacitor assuming the role of the particle displacement, C the mass, and $1/L$ the coupling. Only the gain and loss elements are included for simplicity, with the gain implemented by the negative impedance converter shown in Fig. 1(c). The gain/loss parameter is $\gamma = R^{-1}\sqrt{L/C}$. The net power conducted out of either bath can be obtained from the voltages sampled on the respective source resistance. For example, if $V(t)$ is the voltage on the upper end of the left bath resistance r [see Fig. 1(b)], the power conducted out of that bath is $W_n = \langle V(t)(V_n(t) - V(t)) \rangle / r$. A negative power would indicate heat flux into the bath.

V. CONCLUSIONS

We have demonstrated that heat transport in active harmonic chains can exhibit unique characteristics. The NESS solution was found and studied in detailed. For the case of $\mathcal{PT}$-symmetric arrangements of the active elements, the domain of its existence (with respect to the amplification and attenuation parameter) was maximal. We have found that the heat flux has negative differential thermal conductance, it is independent of the temperature of the bath that is on the other end of the chain, and it shows a nonreciprocal behavior with respect to the two baths.

[1] F. Bonetto, J. L. Lebowitz, and L. Rey-Bellet, in *Mathematical Physics* 2000, edited by A. Fokas, A. Grigoryan, T. Kibble, and B. Zegarlinsky (London, Imperial College London, 2000).

[2] S. Lepri, R. Livi, and A. Politi, Phys. Rep. **377**, 1 (2003).

[3] A. Dhar, Adv. Phys. **57**, 457 (2008).

[4] M. Terraneo, M. Peyrard, and G. Casati, Phys. Rev. Lett. **88**, 094302 (2002); B. Li, L. Wang, and G. Casati, *ibid*. **93**, 184301 (2004).

[5] L. Wang and B. Li, Phys. Rev. Lett. **99**, 177208 (2007).

[6] C. W. Cheng *et al*., Science **314**, 1121 (2006); W. Kobayashi, Y. Teraoka, and I. Terasaki, Appl. Phys. Lett. **95**, 171905 (2009).

[7] T. Prosen and D. K. Cambpell, Chaos **15**, 015117 (2005).

[8] K. G. Makris, R. El-Ganainy, D. N. Christodoulides, and Z. H. Musslimani, Phys. Rev. Lett. **100**, 103904 (2008).

[9] C. E. Ruter *et al*., Nat. Phys. **6**, 192 (2010); T. Kottos, *ibid*. **6**, 3 (2010).

[10] H. Ramezani, T. Kottos, R. El-Ganainy, and D. N. Christodoulides, Phys. Rev. A **82**, 043803 (2010).

[11] C. M. Bender and S. Boettcher, Phys. Rev. Lett. **80**, 5243 (1998); C. M. Bender, Rep. Prog. Phys. **70**, 947 (2007).

[12] C. M. Bender, S. Boettcher, and P. N. Meisinger, J. Math. Phys. **40**, 2201 (1999); C. M. Bender, D. C. Brody, and H. F. Jones, Phys. Rev. Lett. **89**, 270401 (2002).

[13] M. Znojil, Phys. Lett. A **285**, 7 (2001); H. F. Jones, J. Phys. A **42**, 135303 (2009).

[14] O. Bendix, R. Fleischmann, T. Kottos, and B. Shapiro, Phys. Rev. Lett. **103**, 030402 (2009); C. T. West, T. Kottos, and T. Prosen, *ibid*. **104**, 054102 (2010).